RESEARCH PAPER

The Assessment of Second Pulse Effects on the Microstructure and Fracture Behavior of the Resistance Spot Welding in Advanced Ultrahigh-Strength Steel TRIP1100

I. Hajiannia[1,*], M. Shamanian[1], M. Atapour[1], R. Ashiri[2] and E. Ghassemali[3]

*i.hajiannia@ma.iut.ac.ir

[1] Department of Materials Engineering, Isfahan University of Technology, Isfahan, Iran.

[2] Department of Materials Science and Engineering, Dezful Branch, Islamic Azad University, Dezful, Iran.

[3] School of Engineering, Jönköping University, Jönköping, Sweden.

Abstract: *In this study, the effects of the second pulse resistance spot welding on the microstructure and mechanical properties of transformation induced plasticity 1100 steel were evaluated. The thermal process after welding was designed to improve metallurgical properties with pulse currents of 6 kA, 9 kA, and 12 kA after initial welding with 10 kA current. The effect of the second pulse on mechanical and microstructural properties was investigated. The fracture of the welds was for pulsed samples of 6 kA and 9 kA pull out with mechanical test. Due to the existence of the microstructure including the equiaxial dendritic and finer in fusin zone in the pulsed current of 9 kA, the maximum fracture energy, and maximum force were observed. A significant decrease in the FZ hardness in 6 kA current was observed in the nano-hardness results, which was attributed to the existence of martensitic and ferrite temper. The highest ratio of CTS/TSS was obtained for 6 kA and 9 kA, respectively, and force-displacement evaluation was maximum in 9 kA. The fracture surfaces included dendrites and dimples. The results of partial fracture revealed separation in the coherent boundaries of the coarse grain of the annealed region.*

Keywords: *Resistance spot welding, Second pulse current, Fracture surface, Shear tensile, Dendritic microstructure.*

1. INTRODUCTION

The continuous development of advanced high-strength steels (AHHSs) for combining high strength and high ductility with suitable impact resistance for automobile applications requires the study of weldability [1]. Automobile manufacturers should improve the fuel efficiency and safety standards of their vehicles [2]. To address the above issues, it's very important to design and select a material with high strength, formability and also good weldability [3]. Thus, transformation induced plasticity (TRIP) steels have received widespread attention for automotive application due to their excellent combination of strength and ductility. The microstructure of these steels consists of ferrite, bainite, martensite and more than 5% of retained austenite. The retained austenite is the most important phase in TRIP

steel because its strain-induced transformation to martensite during deformation causes work hardening of steel, which delays the onset of necking and eventually leads to a high ductility [4].

The main method used for sheet metal joining in the automobile industry is the resistance spot welding (RSW). This is because of its reliability, fastness, and suitability for automation [5]. The alloy content and high strength of AHSSs limit their weldability and often fracture modes with low-bonding energy are seen. In general, in the RSW, there is a critical weld nugget size, where the fracture mode changes from the low-energy interface fracture (IF) to the ductile peripheral fracture or pull out (PO) mode [6].

In recent years, studies have been done on the pulsed welding and heat treatment after welding on TRIP steels. For example, Balltazar Hernandez et al. [7], performed resistance spot welding

I. Hajiannia, M. Shamanian, M. Atapour, R. Ashiri and E. Ghassemali

on TRIP 800 steel by two pulses of current. Their results showed that tensile shear behavior has improved. In another study Sajjadi Nikoo et al., [8], examined the effect of three different types of post weld heat treatment on the TRIP 700 steel resistance spot welds. Their results showed that according to the applied pulse level, the mechanical properties of the weld are affected by mechanisms such as hardness reduction in the FZ due to the tempering of martensite. Eftekhari et al., [9] investigated the effects of single-pulse and double-pulse on the microstructure of TRIP 980 resistance spot welds. Their results showed that in the second pulse and with the current lower than the first pulse, the size of prior austenite grains has a significant effect on the mechanical properties of lath martensite structures.

In the previous research, the welding cycle, holding time and welding time were at a higher level and pulse current level were very low [6-8]. In this study, it was tried to reduce the time, to produce thousands of welding spots for the automobile body, reducing the welding time that will increase the production efficiency.

2. MATERIALS AND METHODS

In the present study, an uncoated sheet of cold-rolled TRIP1100 steel with a thickness of 1 mm was used as the base metal (BM). The chemical composition and mechanical properties of the BM are listed in Table 1 and Table 2, respectively.

According to the mechanical strength, TRIP 1100 steel sheet is placed in the ANSI / AWS / SAE / D8.9 standard [10]. According to this standard, Copper, Chrome, Zirconium RWMA electrode were chosen for welding operations. With reference to the thickness of the sheets, an electrode with 6 mm diameter was used. TRIP1100 steel sheets were prepared for welding according to AWS D8.9 standard. The welding parameters are listed in Table 3. The microstructural observation was conducted on the cross-section of welded samples using stereographic microscopy, optical microscopy (OM) and scanning electron microscopy (SEM). In this regard, the samples were mounted, mechanically grounded to 1200 grit finish, polished with 0.3 μm alumina suspension

Table 1. Mechanical properties and chemical composition (wt) % for TRIP steel.

Element	C	Si	Mn	S	P	Al	Cr	Ni	CE
Wt.%	0.18	1.03	2.4	0.009	0.003	0.01	0.02	0.3	0.62

Table 2. Tensile properties of TRIP1100 steel used in this study

Yield strength (MPa)	Tensile Strength (MPa)	Elongation (%)
605	1150	23

Table 3. Welding Parameters in Single-Pulse and second-Pulse.

Sample	Squeeze Time (Cycle)	Weld Time 1 (Cycle)	Cool Time (Cycle)	Weld Time (Cycle)	Hold Time (Cycle)	Primary Weld Nugget Size (Mm)	Secondary Weld Nugget Size (Mm)
Single Pulse 10kA (W1)	8	11	8	-	-	5.7	-
Second Pulse 6kA (W2)	8	11	8	8	8	5.3	3.1
Second Pulse 9kA (W3)	8	11	8	11	8	5.4	3.9
Second Pulse 12kA (W4)	8	11	8	11	8	-	5.9

and etched with 2% Nital reagent. Microhardness profile of welded samples was measured across the weld using a Buhler micro-hardness tester at a load of 100 g and a dwell time of 10 s.

In order to study the mechanical properties, the tensile-shear and cross-tensile test samples were prepared according to ANSI / AWS / SAE / D8.9 standards. The tensile shear test was carried out at a speed of 10 mm/min. Each test was repeated twice and the mean value was reported.

The fractured specimens of the tensile shear and cross-tensile tests were investigated to determine the type of fracture. Electron backscatter diffraction (EBSD) on a field emission SEM equipped with an EBSD detector combined with the TSL (OIMA) analysis software was used to characterize crystallographic orientations, and phases.

3. RESULTS AND DISCUSSION

3.1. Microstructural Evaluation

Fig. 1 shows the SEM image of the TRIP 1100 steel BM. As it can be seen, the TRIP steel microstructure consists of bainite, martensite, and retained austenite phases in the ferrite matrix. The size of ferrite grains was in the range of 0.5 to 4 μm.

In order to further investigate the microstructure, EBSD investigations were also conducted on TRIP 1100 steel BM. Fig. 2a shows the im-

age quality (IQ) map of this steel. IQ describes the sharpness of Kikuchi patterns at a given point. Therefore, any distortions to the crystal lattice will produce lower quality diffraction patterns. Based on this argument, dark areas in the IQ map were identified as martensite islands at which, due to the highly distorted lattice, Kikuchi patterns are smeared [11]. Bainite also has a higher degree of lattice distortion and a larger density of sub-grain boundaries than polygonal ferrite [12]. Therefore, a lower IQ value is also expected for bainitic areas. The phase map presented in Fig. 2b indicates the presence of retained austenite in the microstructure. Quantitative evaluations by XRD showed a volume fraction of ~ 16% for the retained austenite [13].

The macrostructure of conventional and pulsed samples is shown in Fig. 3. The boundary of the weld nugget and HAZ can clearly be seen in these images. A coarse columnar structure is seen in the FZ of conventional welds (Fig. 3). After applying the second pulse (Fig. 4), the area fraction of large and columnar grains is clearly reduced. This is due to the re-austenitization of a portion of the FZ in the second pulse. In W2 and W3 samples, the re-melted region in the middle of the initial weld is shown with a dashed line in Fig. 4b. The area between the primary and secondary weld nuggets is annealed, and according to the second level of the pulse, the current is different in size and microstructure for different welds [14]. The comparison of the diameter of the second weld
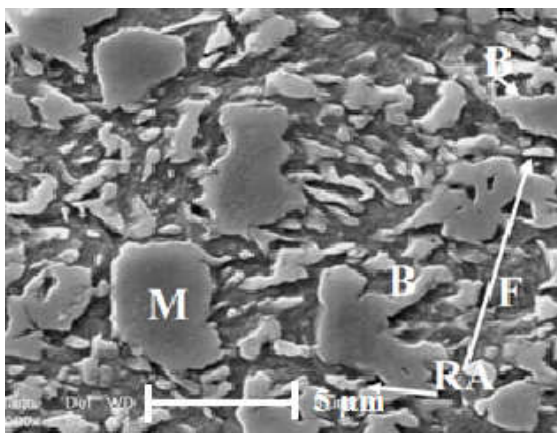

Fig.1. SEM image of TRIP1100 steel BM. B: Bainite, F: Ferrite, M: Martensite, RA: Retained Austenite.
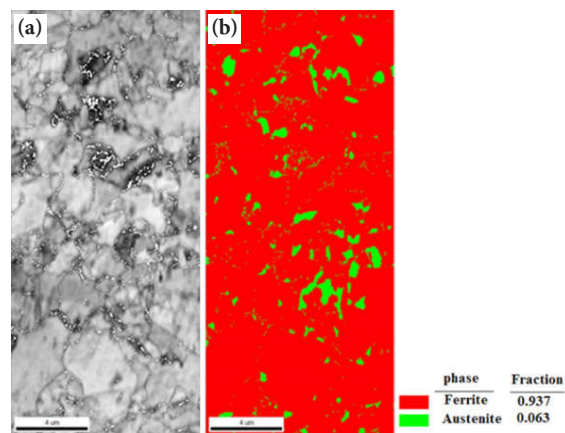

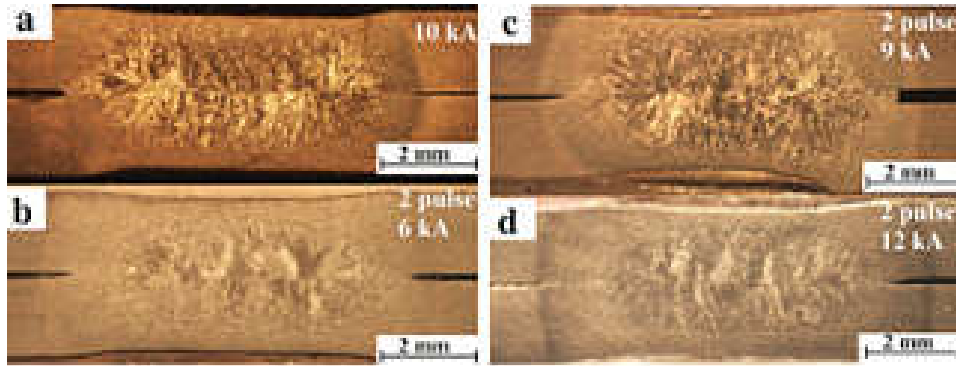**Fig. 2.** (a) IQ map and (b) phase map of ferrite and austenite in the TRIP1100 steel BM.

Fig. 3. Macrographs of the cross sections of the resistance spot welded samples (a) W1, (b) W2, (c) W3, (d) W4.
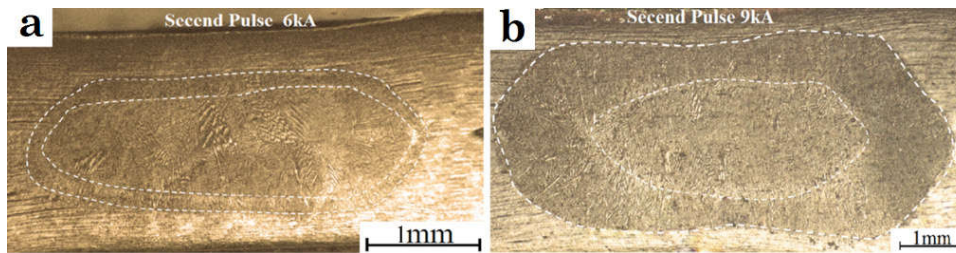

Fig. 4. Macrographs of the cross sections of the resistance spot welded samples (a) W2, (b) W3, The center of the button (nugget) is separated from the primary welding with a dashed line.
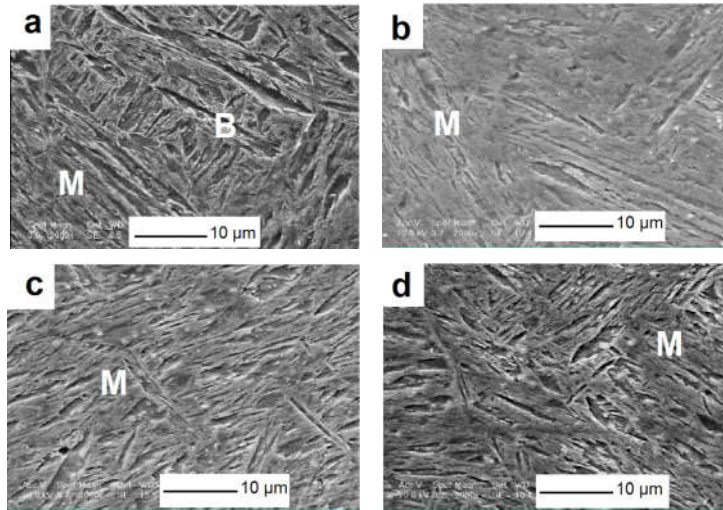

Fig. 5. Resistance spot welding microstructure, a). W1, b). W2, c). W3, d). W4, B, bainite, F, ferrite, M, martensite.

nugget with the primary weld nugget is presented in Table 3. It has been shown that the diameter of the second weld nugget increases with the second current pulse increase.

Fig. 5 (a-d) represents a SEM picture of single- and second-pulse weld structures. Single-

and second-pulse welding microstructure are completely martensite, although some ferrite and feather-shape or above bainite have been found in the structure of the weld.

In Fig. 6, a picture of the region of the welded pulse that includes the initial weld is shown.
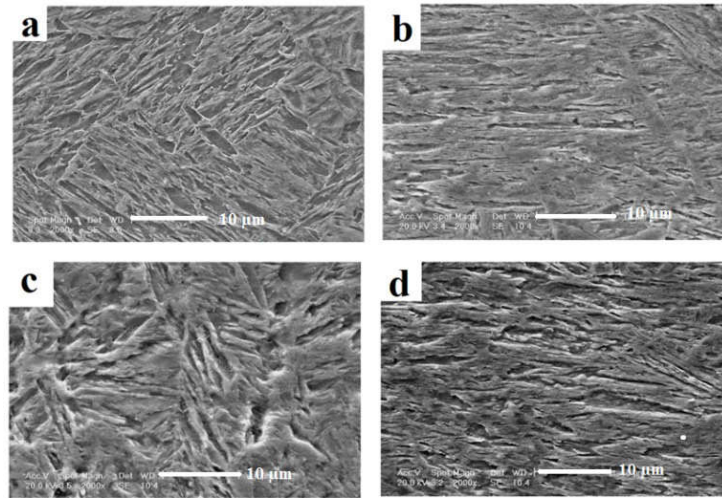
Fig. 6. The microstructure of the pulse welding adjacent annealed region, of resistive spot welding, a). W1, b). W2, c). W3, d). W4.

In this region, the initial welding temperature, which has a microstructure including martensite and some bainite, has increased to a temperature above the AC3 and then cooled [15]. The SEM image in Fig. 6b shows the tempered structure along with the remained ferrite in this area. In the W3, the grains are completely equiaxed and separation of the annealed region is difficult. In the annealed region, grains' stretching and being finer can be determined. Also, tempered martensite packs with a different orientation, approximately equiaxed, are seen in Fig. 6c. In W4, the aniline area was created just after the weld nugget and has large coarser polygonal structures, and the martensite packets are formed adjacent to each other with different orientations after the annealed grains toward the weld

center [16]. In the SEM image of Fig. 6d, it can be seen that the martensite is getting fine and the alignment of martensite to the single-pulse current at the adjacent welding.

3.2. Mechanical Properties

3.2.1. Macroscopic Fracture of the Welds under Tensile Shear and Cross-Tension

Fig. 7 shows the type of single-pulse and second-pulse welds produced by the tensile shear and cross-tension test for TRIP1100 steel. Rotation of the weld nugget is in the direction of thickness, which extends the joint seam in parallel with the growth of cracks and width. It is shown in some sources that
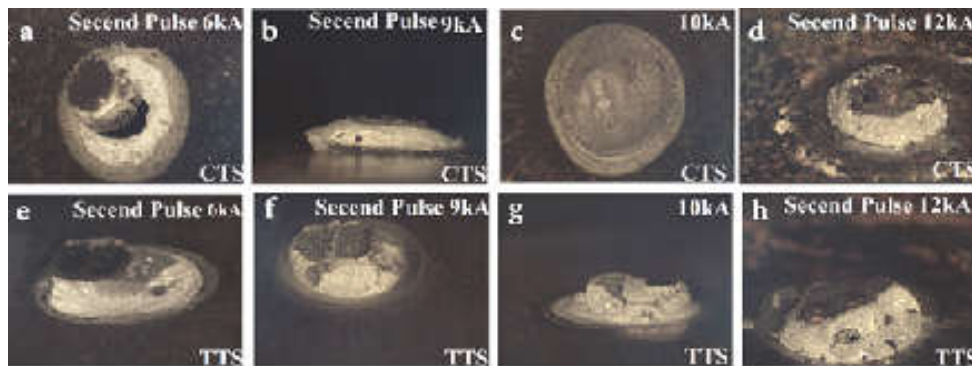

Fig. 7. Macroscopic topography from pulse welding and single pulse fracture type after tensile shear strength (TSS) in the down (e-h) and cross-tension strength (CTS) in up (a-d).

the HAZ zone at the edge of the weld nugget passes upper critical heat affected zone which has high hardness and goes up to the beginning of the weld nugget and slips are continued in the vertical direction with the fracture until failure occurs [20].

Fig. 7 shows the fracture of samples under cross-tension. In this type of tension, the crack traverse moves from the joint groove in the weld nugget environment [21]. Fractures resulting from cross-tension of pulsed samples showed Pull out fracture type, which is due to the joining of grain boundaries in the HAZ region, adjacent to the weld nugget. It is determined that the hardness of the weld nugget and the lower HAZ region, then increase of the desire to pull out failure in cross-fracture. Failure modes for W2 with a lower hardness were almost a pull-out fracture (PO) [22]. For all samples, a thickness and pull out separation were obtained, which was accrued by repeating the test in HAZ fracture zone and ruptured area. In the region that is located in upper critical heat affected zone or UCHAZ, and annealing is accrued and a thermal weld higher than Ac_3 is experienced.

3.2.2 Results of Shear Stretching and Cross-Stretching Tests

Results of Tensile shear and cross-tension test in single-pulse and second-pulse are shown in Table 4. The results of the TSS test indicate that W4 welding has a higher TSS. However, there are not many differences between them. The results have shown the lowest force rate for the W2 and in single-pulse welding, the force rate is greater than W2. From CTS and TSS combination results the ductility ratio is calculated. it has been investigated, which the W2 and W3 second-pulse currents, have the highest amount of ductility, respectively, and the pull out fracture occurred with the CTS test. [24].

Fig. 8. shows maximum force and ductility

ratio (CTS / TSS) in tensile shear strength and cross-tension strength for single-pulse and second-pulse welds the results of the CTS test indicate that CTS in second-pulse welding is higher than single-pulse welding. The highest CTS is related to W2. Figs. 9a and 9b, respectively, show the effect of the second pulse on the displacement in cross-tension, tensile shear and the fracture force rate. As it is obvious, with accomplishing the second pulse, the amount of both displacement and energy absorption have improved about 60%. This improvement, along with the observed microstructure for pulse welds, showed the best situation for the fracture type. Existence of less tightness, along with an almost equiaxed and finer structure, makes brittle martensite flexible and makes the state of the interface closer to peripheral [25].
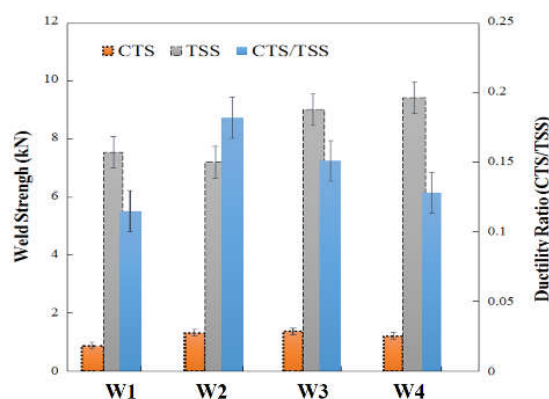

Fig. 8. Maximum force and ductility ratio (CTS / TSS) in tensile shear strength and cross-tension strength for single-pulse and second-pulse welds.

The crack direction initially is seen in the following before austenitic grain boundaries and then as a flexible shear failure in HAZ. In Fig. 9(a-c), a partial fracture microstructure is represented for pulse welding. Figure 9a shows the crack move-

Table. 4. Results of Tensile shear and cross-tension Test in Single-Pulse and second-Pulse.

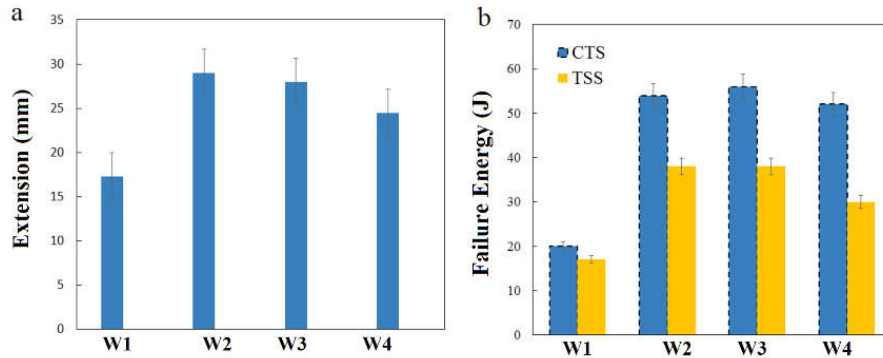| Sample	TSS Maximum Load (N)	CTS Maximum Load (N)	CTS/ TSS	Elastic Modulus GPa
W1	7550 ±15	870 ±8	0.115	210 ±5
W2	7200 ±15	1316 ±9	0.182	173 ±3
W3	9020 ±10	1361 ±5	0.151	170 ±2
W4	9430 ±10	1209 ±10	0.128	212 ±7

Fig. 9. a). Displacement changings diagram for single-pulse and second-pulse samples, b). Weld nugget failure energy change diagram in the tensile shear and cross-tension tensile test.

ment in two interface sheets of existing notches, which occurs as soon as the crack reaches to weld and in the region where there are the first coarse grains from re-austenitization, that has less hardness than the weld. As seen in Fig. 9d, the coherent grain boundary follows the path of crack propagation up to the final failure [28].

Fig. 10. a). Macro image from the fractured section of the tensile shear W3, b). The optical microstructure image of the fracture section, c). higher magnification of the b fractured section and d). The SEM image of the fracture area microstructure of the coarse grains adjacent to the weld with indiscrete boundaries.

3.2.3 Investigation of Fracture Surfaces

Fig. 11 shows the fracture surface's SEM image of a single-pulse welding sample with W1. As shown in Fig. 11a, it shows the failure of W1 sample with a combination of interface and peripheral fracture with about 40% of the interface fracture in the weld nugget.

The SEM image of the W3 weld nugget failure surface is shown in Fig. 12. The weld nugget in Figure 12a is fractured in PO and almost peripheral mode [17]the microstructural characterisation, mechanical testing and fractography investigation were performed on twinning induced plasticity (TWIP. Separation in the weld occurred from its edge at the weld boundary line. Fig. 12 shows the weld nugget adjacent detachment in the annealed region, which includes equiaxed cavities and dimples that are fractured and separated ductility. In Fig. 13d, fracture adjacent to the weld in-
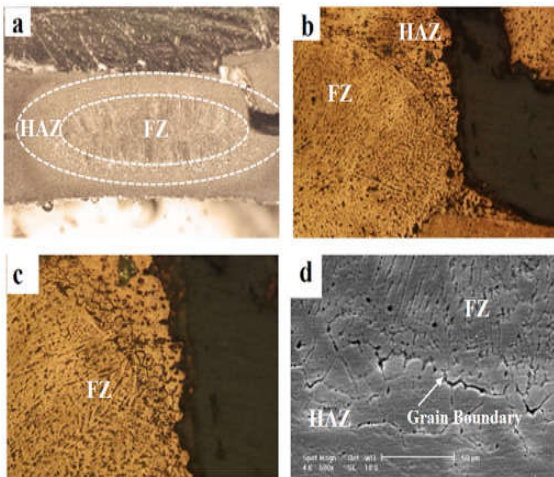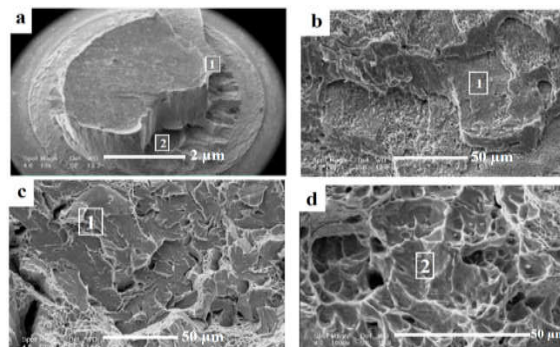

Fig. 11. Fracture surface microstructure by SEM of W1, a) fractured weld nugget in the tensile shear test, b) cleavage fracture by rotation in the weld nugget, c) higher magnification, of Fig. 11 b, d) swirled dimples in the width of weld nugget.

85

cludes dendritic solidification of grains and its growth orientation is so clear. In W2 and W3 second pulse currents, the crack propagation will not begin from the joint seam. And according to Fig. 10, as soon as it reaches to the weld region, changes its path with regard to re-austenitic grains which converted from columnar mode to half equiaxed mode. Also due to temper in the welding region, its hardness decreases and the failure toughness improves [18]fine-grained, and inter-critical zones, and the volume fraction of martensite in HAZ was higher than that in the DP600 base metal (BM. The failure in sheet thickness and in the annealed region occurs in the form of intergranular with coarse grains, and at the weld center, PO detachment is observed.
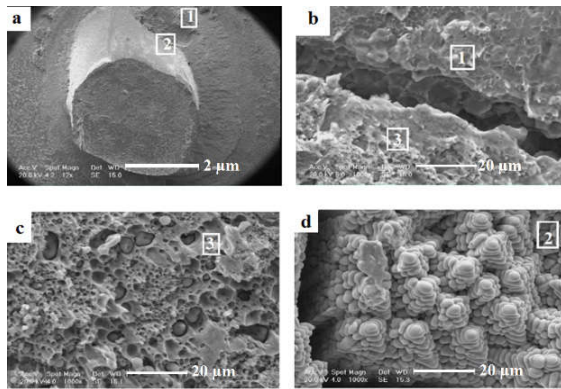

Fig. 12. Microstructure of fracture surface by SEM of W3, a) fractured weld nugget in the tensile shear test, b) intergranular fracture by rotating the weld nugget, c) expansion of the crack adjacent to weld in the annealed zone, d) shear layers in sheet thickness.

3.2.4 The Hardness Tests

The hardness profiles of welds are shown in Fig. 13a. According to the figure, it has been identified that HAZ of pulse welding, in particular in W4, due to an increase in the heat input, it is more extensive than a single pulse and second pulse welding with less current (about 150 micrometer). The hardness rate at the welding center was approximately the same for the W4 and W1, and the nano-hardness observations also showed this result. It can be understood that hardness in adjacent (annealed region) to the pulsed welds decreased by about 12% in comparison with FZ. In W3 in UCHAZ region,

the hardness increasing rate is approximately equal to the 10 kA single-pulse current [37]. The decrease of welding hardness in W2 was higher than other currents, which was attributed to the martensite tempering due to a lower temperature than the primary weld.

The average amount of elastic modulus, calculated by the software and the nano-harness results are presented in Table 4 in W2 and W3 samples with the second pulse, the elastic modulus was lower than single pulse. which it can be Due to transformed martensite to cementite and ferrite tempered.

As shown in Fig. 13b, the rate of indentation in constant load was respectively higher for samples of W2 and W3 with a second pulse than other samples, which is due to the softening of the FZ tempering. Also, the single-pulse W1 and W4 almost have the same hardness on a nano scale.
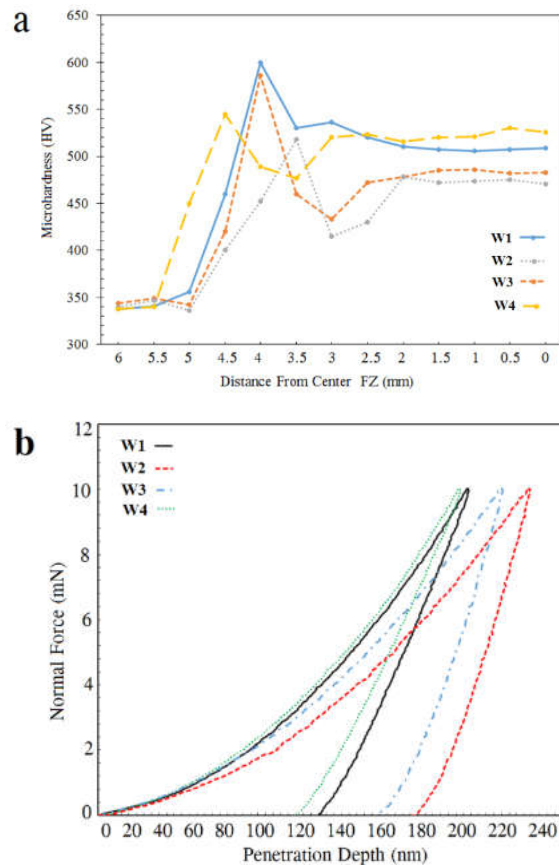

Fig. 13. a) Single-pulse and second-pulse welding hardness profiles, b). Load curve in terms of the height of the penetration depth of the TRIP steel resistance spot welding without the pulse and the second pulse.

4. CONCLUSIONS

Based on the results obtained in this study, we can conclude:

1. Microstructural changes in welding produced by the second pulse showed that with increasing the second pulse current up to less than the initial current, the microstructure consists of approximately equiaxed dendrites with finer grains than the initial welding. Also adjacent to the pulsed weld, an annealed region with microstructure with different martensite blocks were created for different samples.

2. Investigations on the partial failure of the tensile shear strength test (TSS) showed joining of annealed region boundaries, adjacent to the weld, for pulsed samples. In the pulse current of 9 kA, the equiaxed and smaller grain size rate was more than other samples and was similar to the center of FZ sample, whose resulted structure caused the mechanical properties and failure states' improvement in 9 kA pulse current. However, the results showed that the highest CTS was related to the 6 kA second-pulse current. But for 9 kA pulse welding, which had more force and displacement, it showed dimple mode fraction with the separation of dendrites in the crack. Failure for all pulse samples in CTS was PO mode.

3. It was found that HAZ of pulse welding with 12 kA current is wider than other samples due to the increase in entrance heat. In UCHAZ of all samples, hardness was more than welding. Also, the results of nano-hardness showed that the second pulse current hardness reduction rate was higher for 6 kA and 9 kA, respectively than for other samples.

REFERENCES

1. Eftekharimilani, P., van der Aa, E. M., Hermans, M. J. M. and Richardson, I. M., "The microstructural evolution and elemental distribution of a 3rd generation 1 GPa advanced high strength steel during double pulse resistance spot welding", Welding in the World, 2017, 61, 691–701.

2. Spena, P. R., Matteis, P., Sanchez, A. and Scavino, G., "Strength and fracture of TWIP steel dissimilar weld joints", In Convegno IGF XXII Roma, pp. 109–117, 2013.

3. Xia, M., Tian, Z., Zhao, L. and Zhou, Y. N., "Metallurgical and Mechanical Properties of Fusion Zones of TRIP Steels in Laser Welding", ISIJ International, 2008, 48, 483–488.

4. Hajiannia, I., Shamanian, M., Atapour, M., Ghassemali, E. and Saeidi, N., "Development of Ultrahigh Strength TRIP Steel Containing High Volume Fraction of Martensite and Study of the Microstructure and Tensile Behavior", Transactions of the Indian Institute of Metals, 2018, 71, 1363-1370.

5. Nayak, S. S., Baltazar Hernandez, V. H., Okita, Y. and Zhou, Y., "Microstructure-hardness relationship in the fusion zone of TRIP steel welds," Materials Science and Engineering A, 2012, 551, 73–81.

6. Khan, M. S., Bhole, S. D., Chen, D. L., Biro, E., Boudreau, G. and Van Deventer, J., "Welding behaviour, microstructure and mechanical properties of dissimilar resistance spot welds between galvannealed HSLA350 and DP600 steels," Science and Technology of Welding and Joining, 2009,14, 616–625.

7. Baltazar Hernandez, V. H., Okita, Y. and Zhou, Y., "Second Pulse Current in Resistance Spot Welded TRIP Steel - Effects on the Microstructure and Mechanical Behavior," Welding Journal, 2012, 91, 278S–285S.

8. Sajjadi-Nikoo, S., Pouranvari, M., Abedi, A. and Ghaderi, A. A., "In situ postweld heat treatment of transformation induced plasticity steel resistance spot welds," Science and Technology of Welding and Joining, 2018, 23, 71–78.

9. Eftekharimilani, P., van der Aa, E. M., Hermans, M. J. M. and Richardson, I. M., "Microstructural characterisation of double pulse resistance spot welded advanced high strength steel," Science and Technology of Welding and Joining, 2017, 22, 545–554.

10. AWS standard D8-9 1997.PDF

11. Zaefferer, S., Romano, P. and Friedel, F., "EBSD as a tool to identify and quantify bainite and ferrite in low-alloyed Al-TRIP steels," Journal of Microscopy, 2008, 230, 499–508.

12. Hajiannia, I., Shamanian, M., Atapour, M., Ghassemali, E. and Ashiri, R., "A Microstructure evaluation of different areas of resistance spot welding on ultra-high strength TRIP1100 steel," Cogent Engineering, 2018, 5, 1-24.

13. Tomota, Y., Tokuda, H., Adachi, Y., Wakita, M., Minakawa, N., Moriai, A. and Morii, Y., "Tensile behavior of TRIP-aided multi-phase steels studied by in situ neutron diffraction," Acta Materialia, 2004, 52, 5737–5745.

I. Hajiannia, M. Shamanian, M. Atapour, R. Ashiri and E. Ghassemali

14. Tamarelli, C. M., "AHSS 101: the evolving use of advanced high-strength steel for automotive applications," Steel Market Development Institute, 2011, 1, 42.

15. Tang, Z., Ding, H., Du, L. and Li, L., "Microstructures and Mechanical Properties of Si-Al-Mn TRIP Steel with Niobium," J. Mater. Sci. Technol., 2007, 23, 790–794.

16. Safanama, D. S., Marashi, S. P. H. and Pouranvari, M., "Similar and dissimilar resistance spot welding of martensitic advanced high strength steel and low carbon steel: metallurgical characteristics and failure mode transition," Science and Technology of Welding and Joining, 2012, 17, 288–294.

17. Saha, D. C., Cho, Y. and Park, Y. D., "Metallographic and fracture characteristics of resistance spot welded TWIP steels," Science and Technology of Welding and Joining, 2013, 18, 711–720.

18. Yuan, X., Li, C., Chen, J., Li, X., Liang, X. and Pan, X., "Resistance spot welding of dissimilar DP600 and DC54D steels," Journal of Materials Processing Technology, 2017, 239, 31–41.